Sensors & Diagnostics

PAPER

View Article Online
View Journal | View Issue

Cite this: *Sens. Diagn.*, 2025, **4**, 622

Bimodal sensor employing a novel approach for simultaneous selective detection of Ni^{2+} and biomolecules *via* turn-on fluorescence supported by DFT and molecular docking†

Hazeena Shinziya,[a] Avijit Kumar Das, *[a] Malavika S Kumar,[a] Anish Nag[b] and Malay Dolai [c]

A bimodal sensor, (*E*)-2-(4-(diphenylamino)styryl)-1-methylquinolin-1-ium (**DSM**), was designed and synthesized for the simultaneous fluorescence turn-on detection of Ni^{2+} ion and biomolecules such as ct-DNA, BSA, and ovalbumin. Due to its distinct size and steric properties, **DSM** exhibits different binding modes when interacting with Ni^{2+} and DNA/proteins. The probe **DSM** possesses dual functionalities, allowing it to selectively detect Ni^{2+} at one binding site while interacting with ct-DNA, BSA, and ovalbumin at another. Thus, interactions of **DSM** with Ni^{2+} result in fluorescence enhancement at 377 nm and 400 nm, with a detection limit of 1.53 μM and binding constant of 1.2×10^6 M^{-1}. Moreover, the binding of **DSM** with Ni^{2+} has been demonstrated *via* UV-vis, mass spectra, Jobs plots and DFT analysis. Conversely, binding of **DSM** with ct-DNA, ovalbumin and BSA led to an increase in the fluorescence at 425 nm and 435 nm, respectively, with the detection limit at micromolar (ct-DNA) and nanomolar (BSA and ovalbumin) levels. These interactions have been validated through UV-vis spectroscopy, fluorescence studies, and molecular docking analysis. Thus, this study underscores the potential of **DSM** as a versatile tool for simultaneous detection of both metal ions and biomolecules with a unique bimodal approach.

Received 26th February 2025,
Accepted 11th May 2025

DOI: 10.1039/d5sd00028a

rsc.li/sensors

1. Introduction

The development of various chemosensors to detect different metal ions has garnered notable attention due to their extensive relevance in medical, biological, and industrial applications.[1–3] To date, many researchers have investigated various analytical techniques for detecting different metal ions and anions, including atomic absorption spectroscopy, surface-enhanced Raman scattering, ion-selective electrodes, and inductively coupled plasma mass spectrometry.[4] However, these techniques often involve complex procedures, demand skilled operators, and incur significant costs.[5] Therefore, among the various analytical techniques, colorimetric and fluorescent assays are highly favoured as optical methods, as they provide numerous benefits, such as rapid response and high selectivity and sensitivity. Consequently, for the purpose of detecting different metal ions, a multitude of colorimetric and fluorescent sensors have been created.[6–10]

Across various metal ions, nickel is a vital metal nutrient essential for sustaining human life through different functions involving several nickel-containing enzymes and coenzymes, such as urease, Ni–Fe hydrogenases, and F430.[11] Meanwhile, excess nickel accumulation can adversely affect the respiratory and immune systems, although the exact mechanism of nickel imbalance has not yet been identified. Selective fluorescent probes can be used as cell-imaging reagents to detect trace levels of Ni^{2+} in living systems.[12,13] Selective detection of Ni^{2+} is extremely important, but only a few Ni^{2+}-selective peptide,[14,15] protein,[16] polymer[17,18] and fluorescent sensors have been developed so far.[19–22] The development of chemosensors for selective detection of Ni^{2+} is challenging.

Current research is also focusing on the interactions of ligands with proteins and nucleic acids, as these molecules serve as a model for drug design and cancer treatment.[23] Thus, suitable dye molecules that bind to DNA and protein can be used for the detection of nucleic acids or proteins.[24] The binding interactions of the dye with nucleic acid can be easily understood by the change in the absorption or emission spectra. The relatively low demands and the high

[a] *Department of Chemistry, Christ University, Hosur Road, Bangalore, Karnataka, 560029, India. E-mail: avijitkumar.das@christuniversity.in*
[b] *Department of Life Science, Christ University, Hosur Road, Bangalore, Karnataka, 560029, India*
[c] *Department of Chemistry, Prabhat Kumar College, Purba Medinipur, Contai, West Bengal, 721404, India*

† Electronic supplementary information (ESI) available. See DOI: https://doi.org/10.1039/d5sd00028a

sensitivity of the equipment aid in promoting the fluorometric detection of biomacromolecules as the key method. In this regard, a variety of fluorescent probes are particularly helpful ("light-up probes") since their emission intensity dramatically increases when they form complexes with proteins or DNA.[25]

In this respect, various fluorescent probes whose emission intensity increases significantly upon complex formation with DNA or proteins are especially useful ("light-up probes"). This light up fluorescence technique is commonly applied in biology, biochemistry and also in medicine.[26] Along with the biomacromolecules, several small molecules turn out to be essential within cells, and their concentration in the cellular medium determine function or malfunction of the physiological processes. Thus, we herein developed a multifunctional styryl dye, (*E*)-2-(4-(diphenylamino)styryl)-1-methylquinolin-1-ium (**DSM**), for selective detection of the metal ion Ni^{2+} and biomacromolecules like ct-DNA, BSA and ovalbumin. In this scenario, it has been demonstrated that styryl dyes with a cationic hetarene unit with donor-acceptor sites exhibit favourable properties for DNA sensing.[27–29] Additionally, we have shown that donor (triphenyl amine)-substituted- with acceptor (quinolinium) derivatives **DSM** exhibit favorable photophysical properties, making them suitable as versatile building blocks for fluorescent light-up probes for DNA or protein.[30,31] Although there are reports for the detection of Ni^{2+} and DNA/proteins by developing individual sensors, the simultaneous detection of Ni^{2+} and DNA/proteins by designing a single multifunctional chemosensor like **DSM** is rare (Table S1†). Therefore, here we have combined two types of sensing phenomena in **DSM** that associates with DNA/proteins through the quaternary quinolinium motif and Ni^{2+} through the triphenyl amine part (Scheme 1).

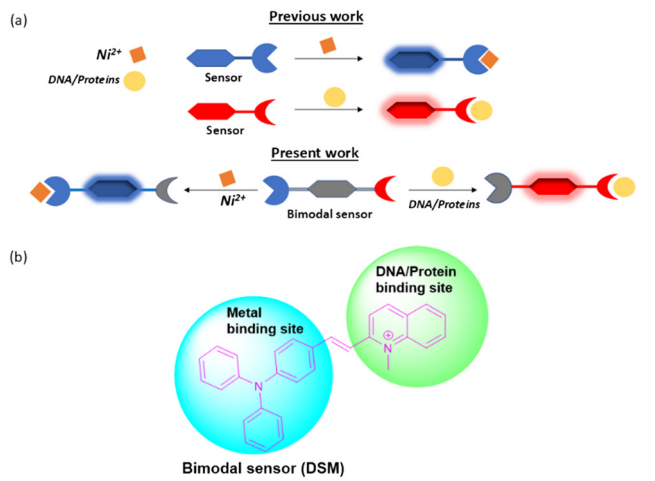

Scheme 1 (a) Simplified cartoon diagram demonstrating the working principle of a dual-mode chemosensor in the present work compared with previous reports. The colored circles represents the fluorescence light-up effect of the molecule. (b) Design of a bimodal senor for simultaneous detection of metal and DNA/protein.

Herein, we have developed a multifunctional sensor (*E*)-2-(4-(diphenylamino)styryl)-1-methylquinolin-1-ium (**DSM**) using Knoevenagel-condensation[32] of 1,2-dimethylquinolin-1-ium (1) with 4-(diphenylamino)benzaldehyde in 66% yield (Scheme 2). The chemical structure of **DSM** was confirmed using ^{1}H-NMR, ^{13}C-NMR, and mass spectrometry (Fig. S9–S11, ESI†).

2. Experimental

2.1 Materials and instrumentation

General. Chemicals, solvents including buffer solution and biomolecules like ct-DNA, BSA and ovalbumin were purchased from Sigma Aldrich. Melting points were determined by utilizing a hot-plate melting point equipment with an open-mouth capillary. On a Bruker Avance 400 MHz instrument, ^{1}H-NMR and ^{13}C-NMR spectra were recorded in DMSO-d_6 solvent. The ^{1}H–^{1}H coupling constants are mentioned in Hz, and chemical shifts are specified in δ-units. UV-vis and fluorescence titration experiments were performed using a UV-spectrophotometer: PerkinElmer, Lambda 30 and a Shimadzu spectrofluorophotometer RF-6000 using a fluorescence cell of 10 mm path, respectively.

2.2 Synthesis and characterization of DSM

Synthesis of 1,2-dimethyl quinolinium iodide was carried out using the reported literature procedure.[33] 2-Methyl quinaldine (0.725 g, 4.5 mmol) was dissolved in ethanol and methyl iodide (9.3 mmol) was added to it. The reaction mixture was then heated to reflux for 48 hours at 80 °C. A yellow-colored precipitate was formed and the precipitate was filtered and dried for the next step without further purification. 1,2-Dimethyl quinolinium iodide (0.208 g, 0.7 mmol) and 4-diphenyl amino benzaldehyde (0.2 g, 7.31 mmol) were dissolved in ethanol (10 ml) and a catalytic amount of piperidine was added to the reaction mixture, which was further refluxed for 24 hours. Reaction progress was monitored by TLC and a red precipitate was formed by the addition of diethyl ether to the reaction mixture. The red precipitate was further purified *via* column chromatography using 2–3% methanol in chloroform as the eluent to obtain a pure red product.

Yield: 200 mg, 66%. Mp-135–140 °C. ^{1}H NMR (DMSO-d_6, 400 MHz): δ (ppm): 8.51 (d, 1H, J = 9.2 Hz), 8.33 (d, 2H, J = 8

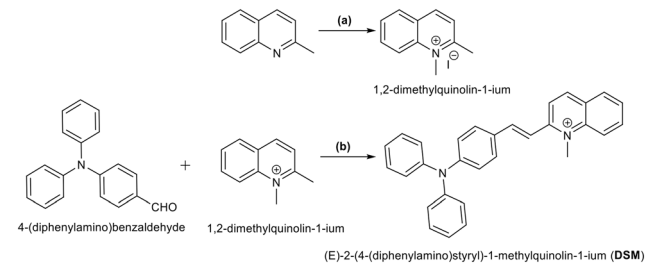

Scheme 2 (a) Methyl iodide and ethanol refluxed at 50 °C, 48 h. (b) Piperidine and ethanol refluxed at 70 °C, overnight.

Hz), 8.21 (d, 1H, J = 15.6 Hz), 8.16 (m, 2H, J = 15.6 Hz), 7.89 (m, 3H), 7.71 (d, 1H, J = 15.6 Hz), 7.42 (t, 4H, J = 7.6 Hz), 7.2 (q, 6H), 6.96 (d, 2H, J = 8.4 Hz), 4.51 (s, 3H). ^{13}C NMR (DMSO-d_6, 100 MHz): δ (ppm): 156.6, 150.9, 147.6, 146.3, 143.6, 139.6, 135.1, 131.6, 130.4, 129.1, 127.9, 127.8, 126.3, 125.5, 121.2, 120.2, 119.6, 116.3. Mass (MS): M^+ calculated for $C_{30}H_{25}N_2^+$ is 413.201; found: 413.250.

3. Results and discussion

3.1 Binding study with Ni^{2+}

The emission properties of **DSM** were studied by adding different interfering metal cations like Cu^{2+}, Hg^{2+}, Al^{3+}, Ni^{2+}, Mn^{2+}, Zn^{2+}, Co^{2+}, Cd^{2+}, Cr^{3+}, Fe^{2+}, Fe^{3+}, and Pb^{2+} (c = 2 × 10^{-4} M) in CH_3CN-HEPES buffer (7 : 3, v/v, pH = 7.4). Initially, **DSM** exhibits two absorption peaks at 331 nm and 497 nm, and results a gradual decrease of absorbance with a moderate shift of wavelength with the incremental addition of Ni^{2+} (Fig. 1a). For **DSM** and **DSM**–Ni^{2+}, the molar absorption coefficients at 497 nm were determined to be 5.3 × 10^4 liter mol^{-1} cm^{-1} and 2.5 × 10^4 liter mol^{-1} cm^{-1}, respectively.

In the emission experiment, the ligand **DSM** itself exhibits a weak emission signal at 400 nm (λ_{ex} = 331 nm) with a quantum yield (Φ = 0.19). With further increase in the concentration of Ni^{2+}, the emission intensity of **DSM** was notably enhanced by 6-fold by the generation of another blue shifted emission peak at 377 nm ($\Delta\lambda$ = 23 nm) along with the ligand signal at 400 nm with a high quantum yield (Φ = 0.76) exhibiting naked eye fluorescence colour change from light orange to blue (Fig. 1c). The decrease of the absorbance and increase of the emission intensity of **DSM** varied up to the saturation level with increasing concentrations of Ni^{2+} (Fig. 1b and d).

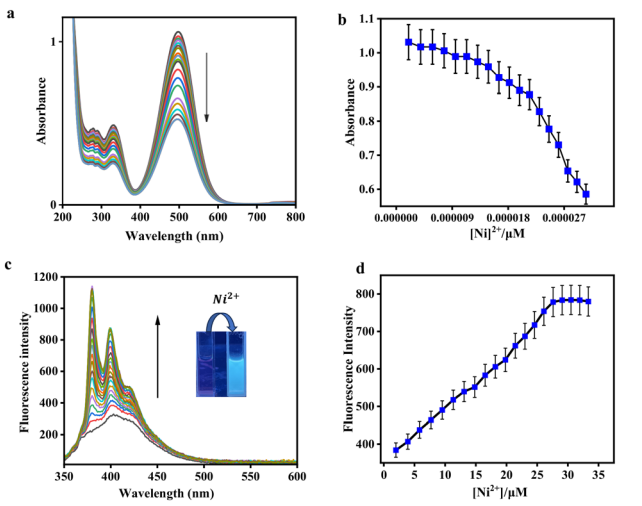

Fig. 1 (a) and (c) UV-vis and fluorescence titration of **DSM** (c = 2 × 10^{-5} M) upon the addition of Ni^{2+} (2 × 10^{-4} M, 10 equiv.) respectively. (b) and (d) changes in concentration *vs.* intensity of **DSM** for Ni^{2+} in UV-vis (λ_{em} = 497 nm) and fluorescence spectra (λ_{em} = 377 nm) respectively.

3.2 Interference study

Fluorescence titration experiments were performed to evaluate the selective binding affinity of **DSM** towards Ni^{2+} in the presence of various metal ions such as Cu^{2+}, Hg^{2+}, Al^{3+}, Ni^{2+}, Mn^{2+}, Co^{2+}, Zn^{2+}, Cd^{2+}, Cr^{3+}, Fe^{2+}, Fe^{3+}, and Pb^{2+} in CH_3-CN–aqueous HEPES buffer (7/3, v/v, pH = 7.4). It is noted that the presence of Ni^{2+} only led to a detectable increase in the fluorescence intensity and no other significant equivalent emission enhancement was observed in the presence of other interfering metal ions (Fig. 2a and b). The bar diagram represents the fluorescence behaviour of **DSM** towards various metal ions with a remarkable selectivity towards Ni^{2+}. The blue bar with the highest intensity indicates the fluorescence enhancement of **DSM** in the presence of Ni^{2+} and orange bars represent no considerable binding of **DSM** with other metal ions (Fig. 2c).

3.3 Competition study

Fluorometric analysis was used to investigate the effect of competing metal ions on **DSM** binding to Ni^{2+} to better analyse the selectivity of **DSM** for Ni^{2+}, where 10 equivalents of Ni^{2+} and other metal ions were used in a cross-contamination study. Notably, the fluorescence enhancement for Ni^{2+} binding remained unperturbed (red bars), and the other interfering metal ions did not affect the sensing of Ni^{2+} (black bars). This indicates that the receptor **DSM** is highly selective and sensitive for Ni^{2+} (Fig. 3).

The detection limit of **DSM** for Ni^{2+} was calculated as 1.53 μM based on the fluorescence titration studies using the formula DL = K × Sb_1/S, where K = 3, Sb_1 is the standard deviation of the blank solution, and S is the slope of the calibration curve (Fig. S4†).[34] The binding stoichiometry was demonstrated through Job's plot analysis showing 1 : 1 binding of **DSM** with Ni^{2+} (Fig. S8†) and the association constant (K_a) of **DSM** with Ni^{2+} was calculated as 1.2 × 10^6

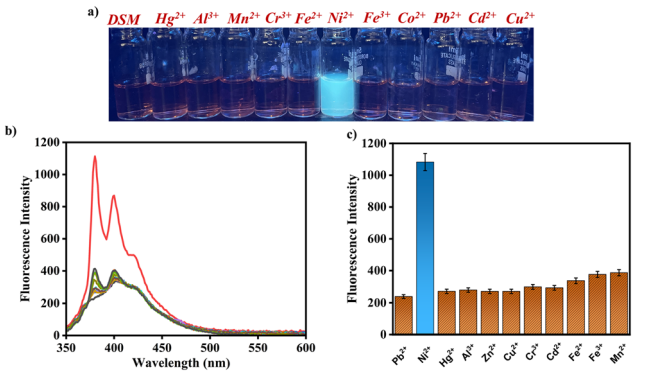

Fig. 2 (a) Fluorescence colour behaviour of probe **DSM** with various metal ions. b) Emission spectra of **DSM** upon the addition of different metal ions (10 equiv.) in CH_3CN–aqueous HEPES buffer solution (7/3, v/v, pH = 7.4) (λ_{em} = 377 nm). (c) Changes in the emission intensity of the sensor **DSM** with the addition of 10 equiv. of each interfering cation (c = 2 × 10^{-4} M, 10 equiv.).

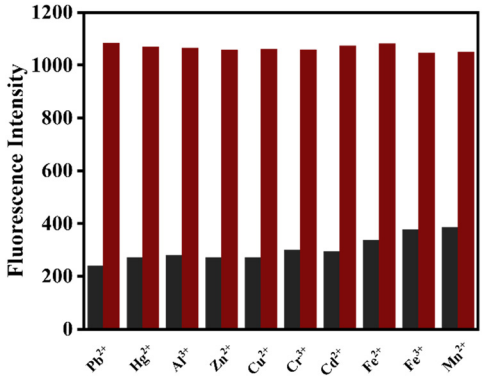

Fig. 3 Change in fluorescence intensity of **DSM** ($c = 2 \times 10^{-5}$ M) on the addition of 10 equiv. of various metal ions ($c = 2 \times 10^{-4}$ M) (green bars); change in fluorescence with the addition of 10 equiv. of various other metal ions in the presence of 10 equiv. of Ni^{2+} at 377 nm (grey bars).

M^{-1} (error <10%) from the fluorescence titration experiment (Fig. S2†).[35]

3.4 Reversibility test

To further explore the binding nature of **DSM** with Ni^{2+}, a fluorescence titration experiment was performed. By adding excess Na_2EDTA (0–2.0 equivalents) to the **DSM**–Ni^{2+} solution, the fluorescence intensity was gradually decreased due to the removal of Ni^{2+} from the metal binding chamber of **DSM** by the strong binding of Na_2EDTA with Ni^{2+} (Fig. 4). The experiment was repeated for several cycles with alternate additions of Ni^{2+} and Na_2EDTA (Fig. S14†). A systematic switching on–off pattern was observed between **DSM** and **DSM** with Ni^{2+} followed by the addition of EDTA. Thus, the reversible binding pattern of Ni^{2+} with **DSM** has been demonstrated.

3.5 Dipstick method

To investigate the practical application of sensor **DSM** towards the sensing of Ni^{2+}, test strips were prepared by immersing the TLC plates into the receptor solution ($c = 2 \times 10^{-5}$ M) in CH_3CN–H_2O (7 : 3, v/v). When **DSM**–Ni^{2+} and **DSM**-coated test strips were exposed to UV light, there was no significant fluorescence observed for the **DSM**-coated test strip (Fig. S13,† left), but the **DSM**–Ni^{2+}-treated test kit exhibited a noticeable turn-on blue fluorescence, which was also observed in the solution phase (Fig. S13,† right). This demonstrates that the test strips, also referred to as dipsticks, selectively detect Ni^{2+} by enhancement of fluorescence which can also be detectable with the naked eye in solid phase. Such dipsticks provide instant qualitative results, eliminating the need for complex instrumental analysis.

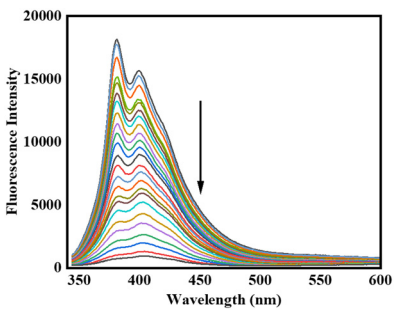

Fig. 4 Fluorescence changes of **DSM** + Ni^{2+} complex solution ($c = 2 \times 10^{-5}$ M) upon the addition EDTA ($c = 2 \times 10^{-4}$ M).

3.6 Probable binding mode in solution phase

Initially, **DSM** alone exhibited weak fluorescence, but a notable fluorescence enhancement was observed at 400 nm in the presence of Ni^{2+}. Since **DSM** is a donor–acceptor type of molecule, there is no significant fluorescence in the absence of Ni^{2+} due to the highly efficient PET process from the donor triphenyl amine moiety to acceptor quinolinium backbone (Scheme 3) (off-state). Significantly, the lone pair of electrons on the nitrogen of the triphenyl amine moiety coordinates with Ni^{2+}, which consequently suppresses the PET process and operates through the chelation enhanced fluorescence (CHEF) effect, which results in notable fluorescence enhancement (on-state).[36] The emission intensity of **DSM** is notably weak ($\Phi = 0.01$), which is likely due to radiationless deactivation of the excited state caused by the isomerization process due to free rotation around the C=C bond, a general phenomenon commonly observed in styryl dyes. Due to co-ordination of Ni^{2+} with **DSM**, C=C bond isomerization was inhibited owing to steric hindrance, which resulted in increased fluorescence intensity of the ligand.[37] This observation can be verified by blocking C=C bond rotation by increasing the viscosity of the solution due to the inhibition of rotational relaxation of the excited molecule (Fig. S1, ESI†).[38] Notably, in highly viscous media with a high proportion of glycerol in methanol, a noticeable rise in fluorescence intensity was observed at 461 nm. Due to the suppression of twisting intramolecular charge transfer (TICT) brought on by conformational changes from rotation around the C=C bond, geometrical rearrangement in the excited state may slow down under high viscosity conditions, leading to enhanced fluorescence. The formation of a complex between **DSM** and Ni^{2+} has been verified through the emergence of a mass peak at $m/z = 582.950$, attributed to [**DSM** + Ni^{2+} + $2Cl^-$ + CH_3CN] (Fig. S12†), which has also been

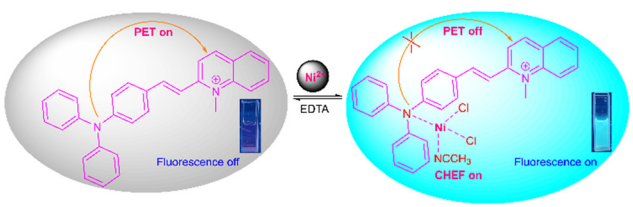

Scheme 3 Probable binding mode of **DSM** with Ni^{2+} in solution phase.

justified by a 1 : 1 binding stoichiometric ratio in the Jobs plot analysis and theoretical calculation.

3.7 Theoretical calculation for Ni^{2+} binding study

The theoretical calculation has been demonstrated through optimization of the **DSM** and **DSM**–Ni^{2+} structures through DFT and TD-DFT calculations. In the optimized structure of the **DSM**–Ni^{2+} complex, Ni^{2+} shows tetrahedral coordination with the charged ligand **DSM** employing four co-ordinations, consisting of one nitrogen from the triphenyl amine group of **DSM**, two from counter anions Cl^- and one from the nitrogen of the acetonitrile solvent. From the optimized structure of the **DSM**–Ni^{2+} complex, the calculated Ni–N (triphenyl amine and acetonitrile nitrogen) bond distances are 1.916 Å and 1.839 Å, respectively, and the Ni–Cl bond distance is 2.171–2.191 Å. Meanwhile, the bond angles of nitrogen and chlorine with Ni are estimated as 176.86° and 175.23°, respectively. Additionally, the HOMO–LUMO energy gap is found to be ΔE = 6.82 eV and 4.97 eV for **DSM** and the **DSM**–Ni^{2+} complex, respectively, indicating their contribution to the stabilization of complex formation (Fig. 5c). Based on the DFT-optimized structures, the total energies of **DSM** alone and the **DSM**–Ni^{2+} complex are 136.55 kcal mol^{-1} and 225.59 kcal mol^{-1}, respectively. Therefore, the energy difference between the **DSM**–Ni^{2+} complex and **DSM** alone is calculated to be 89.04 kcal mol^{-1}. On the other hand, the changes in the absorbance of **DSM** occur upon binding with Ni^{2+} at 330 nm and 490 nm. From the theoretical study, the corresponding estimated absorption bands have been calculated at 329 nm (E = 4.760, f = 0.0079 nm) and 498 nm (E = 3.489, f = 0.1609). For the transition from S0 → S15 and S0 → S2, the experimental data are in good agreement with the theoretical computations; hence, the experimental data align well with the theoretical calculations.

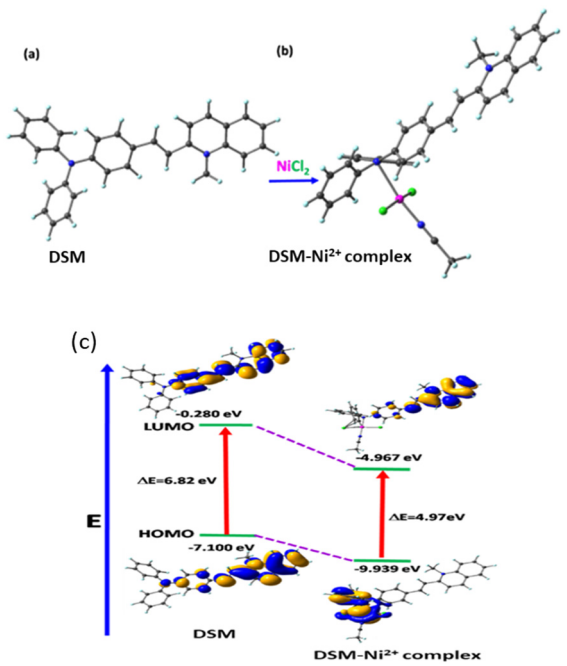

Fig. 5 Geometrically optimized molecular structures of (a) **DSM** and (b) **DSM**–Ni^{2+} complex. (c) Frontier molecular orbital with the energy difference of **DSM** and the **DSM**–Ni^{2+} complex.

3.8 Biological applications

3.8.1 DNA binding study. Utilizing the UV-vis and fluorescence spectroscopy, the relative DNA binding characteristics with **DSM** were examined in Tris-HCl buffer at pH 7.2. Initially, **DSM** itself showed strong absorption signals at 330 nm and 490 nm. The increase in concentration of ct-DNA to **DSM** solution resulted in gradual decrease in absorbance at 330 nm and 490 nm (Fig. 6a). In the fluorescence spectra, **DSM** itself exhibited weak emission at 425 nm with low quantum yield (Φ = 0.01) (λ_{ex} = 330 nm) but progressive addition of ct-DNA to **DSM** caused a gradual increase in the fluorescence intensity at 425 nm by 5-fold with high quantum yield (Φ = 0.02) (Fig. 6c). The spectra undeniably depict the fluorescence turn on behaviour of **DSM** on the addition of ct-DNA. From UV-vis and fluorescence studies, the detection limits of **DSM** for ct-DNA were calculated as 2.79 μM and 1.01 μM, respectively (Fig. S5†). The binding constant (K_b) of 1.2 × 10^4 M^{-1} was determined using the non-linear binding isotherm of **DSM** towards ct-DNA obtained from the fluorometric titrations (Fig. S3a†). The binding study of **DSM** with ct-DNA conducted through photometric and fluorometric experiments unequivocally verifies the binding of these probes with DNA. First, UV-vis titrations revealed a moderate red shift of the absorption band with progressive titration with DNA.[39] The ligand **DSM** has very low quantum yields (Φ = 0.01) with mild

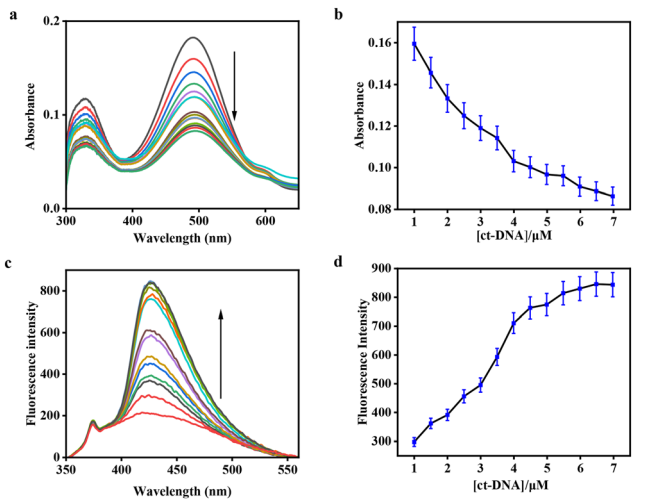

Fig. 6 (a) and (c) UV-vis and fluorescence titration of **DSM** (c = 2.0 × 10^{-5} M) upon incremental addition of ct-DNA (c = 2 mM in base pairs) in Tris-HCl buffer, pH 7.2. (b) and (d) Changes in concentration *vs.* intensity in UV-vis (λ_{em} = 490 nm) and fluorescence spectra (λ_{em} = 425 nm).

fluorescence when DNA was not present in aqueous buffer solution due to radiationless deactivation by conformational relaxation of the excited state. The association with ct-DNA results in the enhancement of emission intensity (Fig. 6c). It has been shown that several DNA sensitive probes exhibit fluorescent light-up effects due to the result of the restricted conformational freedom of movement of the ligand within the binding site,[37] which is also comparable with the fluorescence enhancement observed in highly viscous media like glycerol.[38] Therefore, we propose that the emission enhancement of **DSM** in the presence of DNA is the result of restricted conformational flexibility that reduces the radiationless de-activation of the excited state, which has been demonstrated in a similar study using several styryl- and stilbene-type dyes.[27–29] The steric protection and delocalization of the amino group's lone pair limit its availability, making ligand **DSM** association primarily driven by attractive dispersion interactions like π stacking and van der Waals forces, along with the release of the thermodynamically favorable counter-ion from DNA. Additionally, the structural flexibility of **DSM**, with its hydrophobic triphenylamine and DNA-binding quinolinium backbone, may cause its bulky diaryl unit to point outside the binding site when the charged quinolinium moiety intercalates into DNA.[39]

3.8.2 Ethidium bromide (EB) competition assay. To further investigate the interaction mode between ct-DNA and **DSM**, the quenching assay was employed mainly by the displacement of the intercalating dye (EB) from ct-DNA. When EB is intercalated into the base pair of ct-DNA, it shows a significant increase in the fluorescence intensity. However, the incorporation of a second ligand which can substitute the ct-DNA bound EB or break the secondary structure of DNA results in a decrease of the fluorescence intensity.[40]

Herein, the EB replacement assay has been performed by the fluorescence experiment in Tris-HCl buffer, pH = 7.2. Initially, high fluorescence intensity has been observed for EB bound ct-DNA at 627 nm, which was significantly quenched with the increase in concentrations of the compound **DSM**. This fluorescence quenching is mainly due to the replacement of EB from EB bound ct-DNA complex by **DSM**. This confirms the intercalation binding mode of **DSM** with ct-DNA.[41]

By using the linear Stern–Volmer equation, the quenching of fluorescence in ct-DNA bound EB can be well understood, in which **DSM** is the quencher:[42]

$$I_0/I = 1 + K_{sv}Q$$

where I_0 and I indicate the fluorescence intensities in the presence and absence of the compound **DSM** (quencher), respectively; K_{SV} is the linear Stern–Volmer quenching constant; and Q is the concentration of **DSM**. The ratio of the slope to the intercept gives the K_{SV} value. The K_{SV} value was found to be 6.3 × 10^3 M^{-1}. L, which explains the high quenching efficiency of **DSM** (Fig. 7).

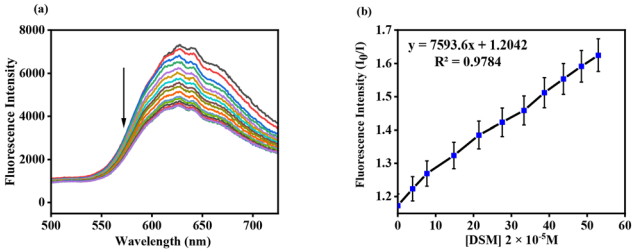

Fig. 7 (a) Fluorescent changes that occur when the ct-DNA–ethidium bromide system is titrated with **DSM** (c = 2 × 10^{-5} M) in Tris-HCl buffer, pH = 7.2. (b) Plot of I_0/I *vs.* [**DSM**] for the titration of the compound to the ct-DNA–EB complex.

3.8.3 Protein binding study. Using UV-vis and fluorescence investigations, the binding capacity of **DSM** with bovine serum albumin (BSA) and ovalbumin were examined in Tris-HCl buffer at pH 7.2.

Initially, **DSM** exhibits strong absorption signals at 330 nm and 490 nm. However, increasing concentrations of BSA and ovalbumin results in significant decreases in the corresponding absorption signals (Fig. 8a and 9a). In the fluorescence experiment, **DSM** exhibited weak emission signal in the absence of BSA and ovalbumin at 425 nm with very low quantum yield (Φ_0 = 0.01). However, incremental increases in the concentration of BSA and ovalbumin to the **DSM** solution resulted in the enhancement of fluorescence intensities by 3-fold at 435 nm and 425 nm with comparatively high fluorescence quantum yields at Φ = 0.02 and Φ = 0.13, respectively (Fig. 8c and 9c). The detection limits of **DSM** for BSA and ovalbumin calculated from UV-vis and fluorescence measurements are 7 nM, 5 nM and 17 nM, 5 nM, respectively (Fig. S6 and S7†). The binding constants of

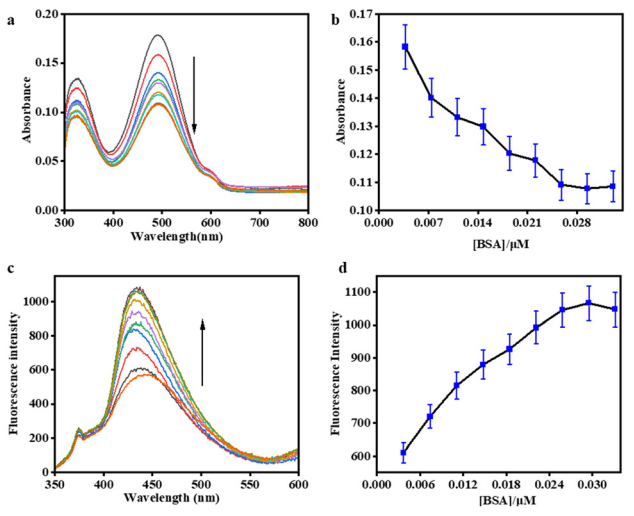

Fig. 8 (a) and (c) UV-vis and fluorescence of **DSM** (c = 2.0 × 10^{-5} M) upon titration with BSA (c = 7.4 μM) in Tris-HCl buffer at pH 7.2 respectively. (b) and (d) Changes in concentration *vs.* intensity in UV-vis (λ_{em} = 490 nm) and fluorescence spectra (λ_{em} = 425 nm) respectively.

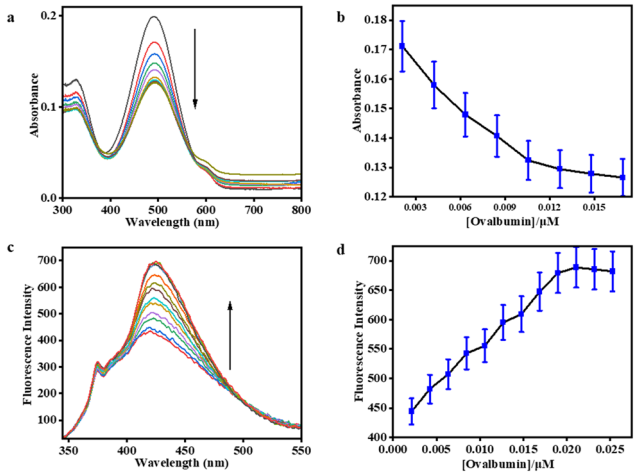

Fig. 9 (a) and (c) UV-vis and fluorescence of **DSM** (c = 2.0 × 10^{-5} M) upon titration with ovalbumin (c = 4.24 μM) in Tris-HCl buffer, with pH = 7.2. (b) and (d) Changes in concentration *vs.* intensity in UV-vis (λ_{em} = 490 nm) and fluorescence spectra (λ_{em} = 425 nm).

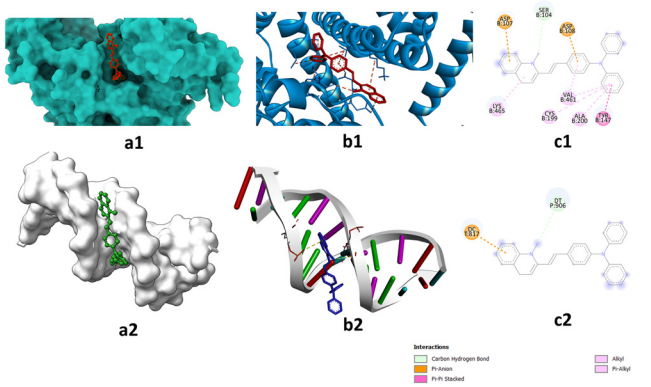

Fig. 10 Possible binding mechanisms of **DSM** with BSA (1), and ct-DNA (2). Three-dimensional surface (a1 and b2) and ribbon (b1 and b2) views of the complex of **DSM** with BSA and ct-DNA, respectively; c1 and c2 represent two-dimensional interaction of BSA and ct-DNA with **DSM**, respectively.

DSM with BSA and ovalbumin obtained from non-linear fitting curves from spectrofluorometric titrations are 1.2 × 10^4 M^{-1} and 5.4 × 10^5 M^{-1}, respectively (Fig. S3b and c†).

The same mechanism that explains the fluorescence light-up effect in the presence of proteins also explains the association of **DSM** with nucleic acids. This mechanism involves a combination of restricted conformational freedom of the molecule and suppressed formation of an ICT or CS excited state within the binding site. The variation of absorbance and the fluorescence response of **DSM** on binding with DNA and proteins is due to the different polarity of the binding cavities and the CS or ICT state is stabilized more proficiently inside the more polar DNA binding cavity compared with the less polar proteins (BSA and ovalbumin) binding pocket.[43,44] The comparatively significant light-up effect in the presence of proteins resulted in a decrease of the CS or ICT state within the binding site.

3.8.4 *In silico* molecular docking studies. The binding interactions of **DSM** with BSA protein and ct-DNA were further supported by molecular docking studies to predict the binding affinity and sites of **DSM** with biomolecules such as proteins and ct-DNA. The analysis was conducted using Autodock Vina technology (ESI). *In silico* molecular docking is a powerful tool that complements experimental techniques, enhancing the understanding and development of fluorescent ligands for DNA and protein binding. Thus, the molecular docking result showed that the selected ligand **DSM** could bind strongly with the target protein bovine serum albumin (BSA) (binding energy: −8.6 kcal mol^{-1}) and the DNA molecule (binding energy: −8.5 kcal mol^{-1}). The interaction between the protein and **DSM** was stabilized through SER104, ASP107, ASP108, TYR147, CYS199, ALA200, VAL461, and LYS465 (Fig. 10a1–c1). Furthermore, the ligand **DSM** formed a complex with the DNA through an intercalation mode and interacted with deoxyribose cytosine (817) and thymine residues (906) (Fig. 10a2–c2), which was also proven by the ethidium bromide (EB) competition assay.

4. Conclusion

The multifunctional sensor **DSM** was successfully designed and synthesized for the simultaneous fluorescence turn-on detection of metal ion Ni^{2+} and biomolecules such as ct-DNA, BSA, and ovalbumin. The unique structural characteristics of **DSM** allow it to exhibit different binding modes due to its distinct size and steric demands. The bimodal functionalities of **DSM** enable selective detection of Ni^{2+} at one binding site while interacting with ct-DNA, BSA, and ovalbumin at another. The interaction of **DSM** with Ni^{2+} results in fluorescence enhancement, with a specific detection limit and binding constant. Similarly, binding investigations with ct-DNA, BSA, and ovalbumin also show increased fluorescence with the detection limit at the micromolar (ct-DNA) and nanomolar (BSA and ovalbumin) levels. The binding of **DSM** with Ni^{2+} was confirmed through mass spectrometry, Job's plots, and DFT analysis, while the binding interactions with ct-DNA, BSA, and ovalbumin were demonstrated using UV-vis, fluorescence, and docking studies. This study highlights the potential of **DSM** as a versatile probe for detecting both metal ions and biomolecules.

Data availability

The data supporting this article have been included as part of the ESI.†

Conflicts of interest

There are no conflicts of interest to declare.

Acknowledgements

The authors would like to thank Christ University, Bengaluru, for the research facilities and Centre for Research, Christ University, for the seed money grant (grant approval number CU-ORS-SM-24/09). Avijit Kumar Das specially acknowledges State University Research Excellence (SERB-SURE) of the Science and Engineering Research Board (SERB) (File Number: SUR/2022/002461) under the Department of Science and Technology, Government of India, for financial support by the research grant and research fellowship for Hazeena Shinziya.

References

1 V. Raju, R. SelvaKumar, S. K. AshokKumar, Y. Tharakeswar and S. K. Sahoo, *Inorg. Chem. Commun.*, 2019, **101**, 74–80.
2 M. Yang, L. Ma, J. Li and L. Kang, *RSC Adv.*, 2019, **9**, 16812–16818.
3 W. Sik Na, P. Raj, N. Singh and D. O. Jang, *Tetrahedron Lett.*, 2019, **39**, 151075.
4 C. Gao, X. Liu, X. Jin, J. Wu, Y. Xie, W. Liu, X. Yao and Y. Tang, *Sens. Actuators, B*, 2013, **185**, 125–131.
5 H. H. Hammud, S. E. Shazly, G. Sonji, N. Sonji and K. H. Bouhadir, *Spectrochim. Acta, Part A*, 2015, **150**, 94–103.
6 (*a*) D. Maity, D. Karthigeyan, T. K. Kundu and T. Govindaraju, *Sens. Actuators, B*, 2013, **176**, 831–837; (*b*) A. K. Das and S. Goswami, *Sens. Actuators, B*, 2017, **245**, 1062–1125.
7 (*a*) W. Du, R. J. Liu, J. Fang, H. Gao, Y. W. Wang and Y. Peng, *Tetrahedron*, 2019, **75**, 130477; (*b*) S. Goswami, S. Maity, A. C. Maity, A. k. Das, B. Pakhira, K. Khanra, N. Bhattacharyya and S. Sarkar, *RSC Adv.*, 2015, **5**, 5735–5740; (*c*) M. S. Kumar, A. K. Das, Y. Bylappa and A. Nag, *RSC Adv.*, 2025, **15**, 6708–6717.
8 (*a*) T. B. Wei, B. R. Yong, L. R. Dang, Y. M. Zhang, H. Yao and Q. Lin, *Dyes Pigm.*, 2019, **171**, 107707; (*b*) S. Vishnu, A. K. Das, Y. Bylappa, A. Nag and M. Dolai, *Anal. Methods*, 2024, **16**, 8164–8178.
9 Z. Gu, H. Cheng, X. Shen, T. He, K. Jiang, H. Qiu, Q. Zhang and S. Yin, *Spectrochim. Acta, Part A*, 2018, **203**, 315–323.
10 S. C. Lee and C. Kim, *Anal. Sci.*, 2019, **35**, 1189–1193.
11 A. Sigel, H. Sigel and R. K. O. Sigel, *Nickel and Its Surprising Impact in Nature*, John Wiley & Sons, 2007, vol. 2.
12 D. W. Domaille, E. L. Que and C. J. Chang, *Nat. Chem. Biol.*, 2008, **4**, 168–175.
13 E. L. Que, D. W. Domaille and C. J. Chang, *Chem. Rev.*, 2008, **108**, 1517–1549.
14 D. A. Pearce, G. K. Walkup and B. Imperiali, *Bioorg. Med. Chem. Lett.*, 1998, **15**, 1963–1968.
15 A. Torrado, G. K. Walkup and B. Imperiali, *J. Am. Chem. Soc.*, 1998, **3**, 609–610.
16 L. L. Salins, E. S. Goldsmith, M. C. Ensor and S. Daunert, *Anal. Bioanal. Chem.*, 2002, **372**, 174–180.
17 B. Wang, Y. Hu and Z. Su, *React. Funct. Polym.*, 2008, **7**, 1137–1143.
18 (*a*) B. Y. Wang, X. Y. Liu, Y. L. Hu and Z. X. Su, *Polym. Int.*, 2009, **6**, 703–709; (*b*) S. Goswami, S. Chakraborty, A. K. Das, A. Manna, A. Bhattacharyya, C. K. Quah and H.-K. Fun, *RSC Adv.*, 2014, **4**, 20922–20926.
19 (*a*) L. Fabbrizzi, M. Licchelli, P. Pallavicini, A. Perotti, A. Taglietti and D. Sacchi, *Chem. – Eur. J.*, 1996, **21**, 75–82; (*b*) R. K. Pathak, J. Dessingou and C. P. Rao, *Anal. Chem.*, 2012, **84**, 8294–8300.
20 C. Bargossi, M. C. Fiorini, M. Montalti, L. Prodi and N. Zaccheroni, *Coord. Chem. Rev.*, 2000, **208**, 17–32.
21 (*a*) L. J. Jiang, Q. H. Luo, Z. L. Wang, D. J. Liu, Z. Zhang and H. W. Hu, *Polyhedron*, 2001, **20**, 2807–2812; (*b*) R. Joseph, B. Ramanujam, H. Pal and C. P. Rao, *Tetrahedron Lett.*, 2008, **49**, 6257–6261.
22 H. Wang, D. Wang, Q. Wang, X. Li and C. A. Schalley, *Org. Biomol. Chem.*, 2010, **8**, 1017–1026.
23 *Molecular Aspects of Anticancer Drug–DNA Interactions*, ed. S. Neidle and M. Waring, CRC, Boca Raton, FL, 1993.
24 A. Granzhan, H. Ihmels and K. Jäger, *Chem. Commun.*, 2009, 1249–1251.
25 (*a*) G. Cosa, K. S. Focsaneanu, J. R. N. McLean, J. P. McNamee and J. C. Scaiano, *Photochem. Photobiol.*, 2001, **73**, 585–599; (*b*) H. Shinziya, R. S. Menon and A. K. Das, *RSC Adv.*, 2024, **14**, 30631–30646.
26 D. Monchaud and M. P. Teulade-Fichou, *Org. Biomol. Chem.*, 2008, **4**, 627–636.
27 (*a*) R. W. Dirks and H. J. Tanke, *Chem. Biol.*, 2006, **13**, 559–561; (*b*) C. V. Kumar, R. S. Turner and E. H. Asuncion, *J. Photochem. Photobiol., A*, 1993, **74**, 231–238; (*c*) A. K. Das, S. I. Druzhinin, H. Ihmels, M. Müller and H. Schönherr, *Chem. – Eur. J.*, 2019, **25**, 12703–12707.
28 (*a*) V. B. Kovalska, D. V. Kryvorotenko, A. O. Balanda, M. Y. Losytskyy, V. P. Tokar and S. M. Yarmoluk, *Dyes Pigm.*, 2005, **67**, 47–54; (*b*) J.-S. Lee, Y. K. Kim, M. Vendrel and Y.-T. Chang, *Mol. BioSyst.*, 2009, **5**, 411–421; (*c*) D. V. Berdnikova, O. A. Fedorova, E. V. Tulyakova, H. Li, S. Kölsch and H. Ihmels, *Photochem. Photobiol.*, 2015, **91**, 723–731.
29 (*a*) Q. Li, Y. Kim, J. Namm, A. Kulkarni, G. R. Rosania, Y. H. Ahn and Y. T. Chang, *Chem. Biol.*, 2006, **13**, 615–623; (*b*) M. Q. Wang, S. Liu, C. P. Tang, A. Raza, S. Li, L. X. Gao, J. Sun and S. P. Guo, *Dyes Pigm.*, 2017, **136**, 78–84; (*c*) A. Manna and S. Chakravorti, *J. Phys. Chem. B*, 2012, **116**, 5226–5233.
30 (*a*) R. W. Sinkeldam, N. J. Greco and Y. Tor, *Chem. Rev.*, 2010, **110**, 2579–2619; (*b*) T. Deligeorgiev, A. Vasilev, S. Kaloyanova and J. J. Vaquero, *Color. Technol.*, 2010, **126**, 55–80; (*c*) S. Vishnu, A. Nag and A. K. Das, *Anal. Methods*, 2024, **16**, 5263–5271.
31 (*a*) H. Özhalici-Ünal, C. L. Pow, S. A. Marks, L. D. Jesper, G. L. Silva, N. I. Shank, E. W. Jones, J. M. Burnette, P. B. Berget and B. A. Armitage, *J. Am. Chem. Soc.*, 2008, **130**, 12620–12621; (*b*) A. K. Das, H. Ihmels and S. Kölsch, *Photochem. Photobiol. Sci.*, 2019, **18**, 1373.
32 L. F. Tietze and U. Beifuss, *Angew. Chem., Int. Ed. Engl.*, 1993, **32**, 131–163.

33 V. F. Traven, A. V. Manaev, A. Yu. Bochkov, T. A. Chibisova and I. V. Ivanov, *Russ. Chem. Bull.*, 2012, **61**, 1342–1362.
34 M. Shortreed, R. Kopelman, M. Kuhn and B. Hoyland, *Anal. Chem.*, 1996, **8**, 1414–1418.
35 (*a*) H. A. Benesi and J. H. Hildebrand, *J. Am. Chem. Soc.*, 1949, **71**, 2703–2707; (*b*) Y. Shiraishi, Y. Kohno and T. Hirai, *Ind. Eng. Chem. Res.*, 2005, **44**, 847–851.
36 H. Niu, J. Liu, H. M. O'Connor, T. Gunnlaugsson, T. D. James and H. Zhang, *Chem. Soc. Rev.*, 2023, **52**, 2322–2357.
37 R. N. Dsouza, U. Pischel and W. M. Nau, *Chem. Rev.*, 2011, **111**, 7941–7980.
38 M. A. Martin, M. Ballesteros and B. D. Castillo, *Anal. Chim. Acta*, 1985, **170**, 95–100.
39 W. Sbliwa, G. Matusiak and B. Bachowska, *Croat. Chem. Acta*, 2006, **79**, 513.
40 (*a*) J. H. Zhou, S. Q. Xia, J. R. Chen, X. S. Wang, B. W. Zhang, H. J. Zhang, P. Zou, X. Cheng Ai and J. P. Zhang, *J. Photochem. Photobiol., A*, 2004, **165**, 143–147; (*b*) Q. Zhang, F. Zhang, W. Wang and X. Wang, *J. Inorg. Biochem.*, 2006, **100**, 1344–1352; (*c*) Y. F. Song and P. Yang, *Polyhedron*, 2001, **20**, 501–506.
41 D. J. Patel, *Acc. Chem. Res.*, 1979, **12**, 118–125.
42 Y. Chen, M. Cai, Y. Zhang and W. Zheng, *Study on The Mechanism of Chitosan Complex Formation with PEGFPC~ 3 DNA*, Pharmaceutical Biotechnology Beijing, 2005, vol. 5, p. 291.
43 A. Cuervo, P. D. Dans, J. L. Carrascosa and L. Fumagalli, *Proc. Natl. Acad. Sci. U. S. A.*, 2014, **111**, 3624–3630.
44 J. Eden, P. R. C. Gascoyne and R. Pethig, *J. Chem. Soc., Faraday Trans.*, 1980, **76**, 426–434.